Journal of Catalysis 281 (2011) 222–230

Contents lists available at ScienceDirect

Journal of Catalysis

journal homepage: www.elsevier.com/locate/jcat

Investigation of the structure and activity of $VO_x/ZrO_2/SiO_2$ catalysts for methanol oxidation to formaldehyde

William C. Vining, Jennifer Strunk, Alexis T. Bell *

Chemical Sciences Division, Lawrence Berkeley National Laboratory, Berkeley, CA 94720, United States
Department of Chemical and Biomolecular Engineering, University of California, Berkeley, CA 94720-1462, United States

ARTICLE INFO

Article history:
Received 11 March 2011
Revised 29 April 2011
Accepted 1 May 2011

Keywords:
Methanol
Formaldehyde
Oxidation
Vanadia
Ziirconia
Silica

ABSTRACT

High surface area silica-supported bilayered $VO_x/ZrO_2/SiO_2$ catalysts were prepared with a constant vanadium surface density of 0.5 V nm^{-2} and zirconium surface coverages ranging from 0.0 to 2.1 Zr nm^{-2}. In all cases, the zirconia layer was predominantly amorphous in nature. The vanadia existed as isolated tetrahedral O=V(—OM)$_3$ (M = Si, Zr) regardless of zirconia surface density. At least two distinct tetrahedral vanadia environments were identified by ^{51}V NMR on the support: O=V(O—Si)$_3$ and O=V(O—Zr)$_3$, with up to 35% of all V in the latter site at the highest Zr loading. The fraction of V bound to Zr as determined by ^{51}V NMR agrees with an independent determination of the fraction of sites reduced by methanol at 600 K, a temperature too low for significant reduction of vanadia on silica. The turnover frequency for methanol oxidation increased by nearly two orders of magnitude as the Zr loading was increased. When normalized by the number of O=V(O—Zr)$_3$ sites determined from ^{51}V NMR and UV–Visible, the turnover frequency for methanol oxidation to formaldehyde was constant with zirconia surface coverage. It is proposed that the much higher activity of O=V(O—Zr)$_3$ compared with O=V(O—Si)$_3$ sites is attributable to differences in the mechanism by which H-abstraction from V—OCH_3 groups in the rate-limiting step leads to formaldehyde formation associated with the two types of sites.

1. Introduction

The activity of vanadate species for the oxidation of methanol to formaldehyde strongly depends on the composition of the oxide to which these species are bonded [1–3]. Vanadate species dispersed on titania and zirconia, for example, are more than an order of magnitude more active than similar species dispersed on silica, and even higher rates are possible if ceria is used as the support [1,3,4]. Similar effects of support composition have been observed for vanadate species dispersed on silica containing submonolayer coverages of titania or zirconia [4–7]. While a number of proposals have been made to explain the origin of the observed support effects, a consensus concerning the primary cause(s) has not yet emerged [1–5,8–12]. To achieve this goal, it is necessary to characterize, thoroughly, the composition and surface structure of the support. Structural characterization of the supported vanadate species is equally important, since a part of the observed difference in catalytic activity with support composition could be attributable to differences in the structure of vanadate species dispersed on different supports. A particularly fruitful approach for gaining insights into the factors affecting the activity of dispersed vanadate species involves the preparation of two-dimensional submonolayer oxides on silica and subsequent deposition of isolated vanadate species on such supports. This approach is well illustrated in the studies by Wachs and coworkers [6] and our own [4] for vanadate species dispersed on submonolayer deposits of titania grafted to silica, in which V—O—Ti bonds were shown to be responsible for the rate increase through stabilization of the transition state in the rate determining step. In the present study, we have extended our efforts to isolated vanadate species deposited onto submonolayers of zirconia deposited onto silica. The structure of the deposited zirconia layer was characterized by Raman and UV–Visible spectroscopy and by XANES and EXAFS. These techniques, as well as ^{51}V MAS NMR, were used to characterize the dispersed vanadate species. An important finding of our work is that the activity of $VO_x/ZrO_x/SiO_2$ catalysts prepared with a fixed surface concentration of vanadia increases with increasing surface coverage of silica by zirconia. This increase is attributed to the fraction of the vanadate species bonded to zirconia.

2. Experimental methods

MCM-41, high surface area mesoporous silica, was synthesized according to previously reported methods [13–15]. Briefly, dodecyltrimethylammonium bromide (DTMABr) and isopropyl alcohol

* Corresponding author at: Department of Chemical and Biomolecular Engineering, University of California, Berkeley, CA 94720-1462, United States.
E-mail address: alexbell@berkeley.edu (A.T. Bell).

0021-9517/$ - see front matter © 2011 Elsevier Inc. All rights reserved.
doi:10.1016/j.jcat.2011.05.001

were added to a flask and stirred at 313 K until fully dissolved. This mixture was then added to tetraethylorthosilicate (TEOS) in a Teflon container and stirred rigorously at ambient temperature for 30 min. A mixture of tetramethylammonium hydroxide (TMAOH) and de-ionized water was added to the TEOS mixture drop-wise and stirred for 2 h. The resulting mixture had a molar ratio 1:0.75:0.26:84.4 of TEOS:DTMABr:TMAOH:H_2O. The milky-white mixture was heated to 358 K for 4 h, and de-ionized water was added to maintain the liquid level. This mixture was sealed into the Teflon container and placed into an oven at 373 K for 7 days without stirring and was then filtered and rinsed with de-ionized water. The wet powder was heated to 823 K at 2 K min^{-1} in high-purity synthetic air and held at this temperature for 5 h.

The surface areas of MCM-41 and the final catalysts were determined by nitrogen physisorption (Quantachrome Autosorb-1 instrument) using the single point BET method.

Zirconium was grafted onto the silica support using zirconium 2-methyl-2-butoxide (Gelest) as the precursor. The amount of precursor needed to obtain a desired surface coverage was mixed with approximately 60 cm^3 of anhydrous toluene, after which the solution was added to dry MCM-41 and stirred for 4 h at ambient temperature. The solid was filtered from the suspension and then heated in 50 $cm^3(g\ min)^{-1}$ high-purity synthetic air at 4 K min^{-1} to 773 K for 1 h. Multiple grafting steps were used to obtain zirconium surface coverages greater than 0.8 Zr nm^{-2}. Vanadium was grafted onto the samples, after zirconium grafting and air treatment, in a single grafting step, using $VO(O^iPr)_3$ (Alpha, 96% pure) as the vanadium precursor. The procedure for carrying out the grafting of vanadium was analogous to that used to graft zirconium. The weight loadings of Zr and V were determined by inductively coupled plasma emission analysis at Galbraith Laboratories, and the surface densities of Zr and V were determined on the basis of the bare support surface area. Monolayer coverage is approximately 7 M nm^{-2} (M = V, Zr) based on the number of V atoms that can be placed per nm^2 on bulk crystalline oxides.

Raman spectra were acquired using a JobinYvon–Horiba spectrometer equipped with a confocal microscope and a 532 nm Nb/YAG laser. The laser line at 532 nm was removed from the backscattered light using an edge filter, and the filtered radiation was detected by a CCD detector (Andor) after passage dispersion by a grating. Prior to the acquisition of Raman spectra, samples were treated at 773 K in 60 cm^3/min of 20% O_2/He for 1 h, cooled in He (99.999%) flow, and then sealed in quartz tubes. Ten scans of 1 s each were acquired at room temperature using 15 mW of laser power at the sample.

^{51}V nuclear magnetic resonance (NMR) spectra were obtained using an Avance 500 MHz (11.75 T) magnet in the solid-state NMR facility at the University of California, Davis. The samples were pretreated at 773 K for 1 h in 20% O_2/He flowing at 60 cm^3/min. After that, it was cooled and loaded into a 7 mm ZrO_2 rotor under anhydrous conditions. The measured 90° pulse length was 3 μs, and a 1.5 μs pulse length was used to achieve a 45° tip angle. All chemical shifts were referenced to the chemical shift of V_2O_5, −609 ppm [16]. Spectra were acquired using a magic angle spinning (MAS) speed of 7 MHz. Spectra were also recorded at the University of California, Berkeley, using a 300 MHz (7 T) magnet in order to establish that the spectral shapes reflected true chemical shifts and not quadrupolar broadening effects due to vanadium [17].

V K-edge and Zr K-edge XAS measurements were performed at the Stanford Synchrotron Radiation Laboratory (SSRL) on beamlines 4–3 and 4–1 using Si(1 1 1) and Si(2 2 0) monochromator crystals, respectively. All scans were taken in transmission mode using ionization chambers filled with N_2, and a reference foil placed after the sample for energy calibration. The sample mass was adjusted to obtain an absorbance of 2.5, and boron nitride was added, as needed, to form a self-supporting pellet. The sample cell has been described previously [18]. The catalysts were treated in high-purity synthetic air at 773 K for 1 h before cooling in He to ambient temperature. All scans were taken at ambient temperature.

The XAS data were analyzed with the IFEFFIT software and its complementary GUI: Athena [19,20]. The edge energy was defined as the first inflection point after any pre-edge feature. The data were normalized by subtracting a pre-edge line fit to the data from −150 to −30 eV relative to the edge energy and a quadratic polynomial (k weight = 2) fit to the data from 150 to 783 eV relative to the edge energy. A fourth order polynomial spline was fit to the data from 0 to 15.96 $Å^{-1}$ and subtracted to obtain the EXAFS data, minimizing background signals below 1 Å. Finally, the EXAFS data were Fourier transformed from 2 to 11 $Å^{-1}$.

Diffuse reflectance UV–Visible spectra were recorded using a Harrick Scientific diffuse reflectance attachment (DRP) with a reaction chamber (DRA-2CR) and a Varian-Cary 6000i spectrophotometer. The spectra of oxidized samples were acquired at ambient temperature after treating the catalysts in 20% O_2/N_2 at 723 K for 1 h. The edge energy was calculated using Tauc's law for indirect transitions in amorphous and crystalline semiconductors [21]. In this expression, a straight line is fit through a plot of $[F(R_\infty)h\nu]^{1/2}$ versus $h\nu$, where $F(R_\infty)$ is the Kubelka–Munk function and $h\nu$ is the incident photon energy. The x-intercept of this linear fit is the edge energy.

Measurements to determine the fraction of vanadium active for MeOH oxidation were performed in the UV–Visible, using a fully oxidized sample as the reference. A reaction mixture of 8% O_2/4% MeOH/He flowing at 60 cm^3/min was passed over the catalyst at 600 K for 10 min before the reaction mixture was switched to 4% MeOH/He and scans taken every 2 min. The absorbance at 15,000 cm^{-1} was used to indicate the degree of reduction of the V centers on the catalyst. The extent of reduction was determined by comparison to a calibration curve in a manner identical to that done previously [22]. The calibration curve was determined by reducing an equivalent mass of catalyst in the UV–Visible spectrometer at 623 K in 10% H_2/He flowing at 100 cm^3/min and recording the change in its absorbance at 15,000 cm^{-1}. The number of reduced V centers formed was quantified in a separate apparatus using the following technique. A mass of catalyst equivalent to that used for the UV–Visible measurements was reduced at 623 K in 10% H_2/He flowing at 100 cm^3/min and then by pulse reoxidized in 3% O_2/He flowing at 30 cm^3/min. Each O_2 adsorbed was assumed to provide $4e^-$. The calibration curve was generated by plotting the signal of the UV–Visible spectra of these samples with the corresponding time point for total e^- adsorbed per V reoxidized pulsewise in the mass spectrometer. The fraction of V reduced was assumed to correspond to the e^-/V ratio determined from the experiment.

Temperature programmed reaction (TPR_x) experiments were performed using a mixture of approximately 25 mg of catalyst and 25 mg of bare MCM-41 to provide sufficient catalyst bed depth. The mixture was placed in a quartz reactor and supported with quartz wool. The sample was heated at 4 K/min to 773 K in a flow of high-purity O_2 in He (20% O_2/He) flowing at 60 cm^3/min and then held at 773 K for 1 h. Next, the sample was cooled in the synthetic air mixture to 363 K, after which a mixture of 4% MeOH/7.5% O_2/He was flowed over the catalyst for 10 min at 363 K before the reactor temperature was increased from 2 K min^{-1} to 823 K. The reactor effluent was analyzed with a MKS Cirrus mass spectrometer. The concentrations of species formed were analyzed using a matrix-deconvolution method with calibrated response factors.

3. Results and discussion

3.1. Catalyst characterization

Table 1 lists the properties of the materials prepared for this study. The BET surface area of MCM-41 was 1353 $m^2 g^{-1}$. The maximum zirconium loading obtained for a single grafting was 9.45 wt.%, corresponding to 0.8 Zr nm^{-2}. Higher Zr loadings were obtained with repeated grafting steps, and the highest loading, 2.1 Zr nm^{-2}, was obtained after three graftings. Vanadium surface coverages of 0.3–0.6 V nm^{-2} were obtained from a single grafting step. A low vanadium surface coverage was used intentionally in order to prevent the agglomeration of the vanadia, which is known to form V_2O_5 for coverages greater than 0.7 V nm^{-2} on silica [3,23].

Fig. 1 shows Raman spectra of the catalysts after treatment in 20% O_2/He at 773 K. The broad band centered near 485 cm^{-1}, and the peaks at 600 cm^{-1} and 800 cm^{-1} are all indicative of the bare silica support [24]. The shoulder at 1060–1080 cm^{-1} can be attributed to Si—O vibrations [25]. Upon grafting of vanadium onto ZrO_2/SiO_2, a peak appears around 1035 cm^{-1} indicative of the V=O stretch for isolated tetrahedral vanadium species on silica [24]. As the weight loading of Zr was increased, the position of the vanadyl peak shifted from 1040 to 1033 cm^{-1}. This trend is similar to that reported previously for $VO_x/ZrO_2/SiO_2$, in which the vanadyl stretching frequency decreased from 1041 cm^{-1} to 1039 cm^{-1} with increasing zirconium loading [7]. The red shift in the V=O stretching vibration agrees with the observation that the frequency for the V=O stretch for VO_x/ZrO_2 is lower than that for VO_x/SiO_2 [3,26,27]. The appearance of a band at 995 cm^{-1}, indicative of V_2O_5, was not observed [28], further indicating that the vanadium is well dispersed in a tetrahedral coordination on the surface of the support.

At the Zr loading of 1.3 Zr nm^{-2}, a broad peak appeared at 924 cm^{-1}, which has been attributed to the formation of V—O—M (M = V, Zr) bonds in similar systems [7,26]. This band is not observed in the Raman spectra ZrO_2/SiO_2 catalysts regardless of zirconium weight loadings and is present only upon grafting of V. We believe that this peak could be due to V—O—V bonds formed by inadvertent exposure of the sample to moisture during V grafting. No peaks associated with monoclinic or tetragonal zirconia are observed for most Zr surface coverage, indicating that the Zr atoms are well dispersed on the support. The small shoulder at 650 cm^{-1} seen in the spectrum for the highest loading Zr sample (2.1 Zr nm^{-2}) could be indicative of small tetragonal ZrO_2 clusters on the support [29–32], formed during the V grafting process, because this peak is not present in the spectrum of 2.1 ZrO_2/SiO_2. The large silica peak makes it difficult to determine whether additional peaks for *t*-ZrO_2 at 280, 316, or 462 cm^{-1} are present [7]. The amount of tetragonal ZrO_2, if present, is small, however, given the peak size in the Raman spectrum. No bands were observed at 780 cm^{-1} indicative of ZrV_2O_7 units [26] in the final catalysts. Therefore, for all catalysts studied, the Zr and V atoms are well dispersed.

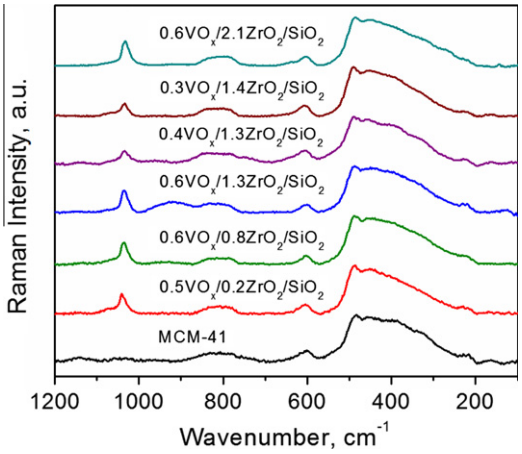

Fig. 1. Raman spectra of $VO_x/ZrO_2/SiO_2$ samples and MCM-41 after treating in high-purity 20% O_2/He at 773 K for 1 h. Scans taken at ambient temperature.

Zr K-edge XANES spectra are shown in Fig. 2. All spectra show the same edge at 18,015 eV, indicating that Zr is present in the 4+ oxidation state regardless of the Zr coverage [33,34]. The small shoulder around 18.001 keV, which is more visible in the inset, is indicative of hybridization between the oxygen p- and zirconium d-orbitals, which occurs for non-centrosymmetric species, and represents a transition from 1s to 4d orbital [32,33]. The intensity of this peak increases with decreasing Zr surface density. Furthermore, as the zirconium surface coverage decreases, the peaks at 18.020 keV and 18.070 keV shift toward higher energy. Both the decrease in intensity of the shoulder at 18.001 keV and the shift in the position of oscillations to lower energy indicate that as the coverage increases the zirconia agglomerates to form domains with increasing oxygen coordination of zirconium to form centrosymmetric structures with a lengthening of the Zr—O bonds [33–36]. Detailed understanding of the Zr bonding environment does not exist in the literature; however, most studies of zirconia–silica gels and supported zirconia indicate that the zirconium atoms have 5 or greater oxygen bonds [7], yet coordination numbers of 5 have been observed in EXAFS for weight loadings less than 17% [37]. Therefore, the observed changes in the Zr K-edge XANES could indicate a shift from 5-coordinate Zr atoms at the lowest loadings to 6 or higher Zr—O coordinations at the highest.

After V grafting, the Zr K-edge shows minor changes that are best illustrated by comparing the derivatives of the normalized Zr K-edge XANES spectra with and without grafted V. As seen in Fig. 3, the greatest changes in the spectra occur for the lowest surface coverage of Zr, which is consistent with larger fractions of Zr

Table 1
Surface area of MCM-41 before and after Zr and V grafting on a metal-free basis and vanadium and zirconium weight and surface coverages for the surface area after metal grafting.

Sample name	V (wt.%)	Zr (wt.%)	MCM-41 surface area ($m^2 g^{-1}$)	Surface area after V and Zr grafting ($m^2 g^{-1}$)	V coverage (V nm^{-2})	Zr coverage (Zr nm^{-2})
0.5VO_x/0.2ZrO_2/SiO_2	4.08	2.68	1350	1040	0.46	0.17
0.5VO_x/0.4ZrO_2/SiO_2	3.85	5.55	1350	960	0.47	0.38
0.6VO_x/0.8ZrO_2/SiO_2	4.16	9.45	1350	800	0.61	0.78
0.6VO_x/1.3ZrO_2/SiO_2	4.07	15.4	1350	800[a]	0.60	1.30
0.3VO_x/1.4ZrO_2/SiO_2	2.25	17.9	1350	860	0.31	1.40
0.4VO_x/1.3ZrO_2/SiO_2	3.04	16.7	1350	820	0.44	1.30
0.6VO_x/2.1ZrO_2/SiO_2	3.65	23.2	1350	720	0.60	2.13

[a] Surface area approximated based on other samples.

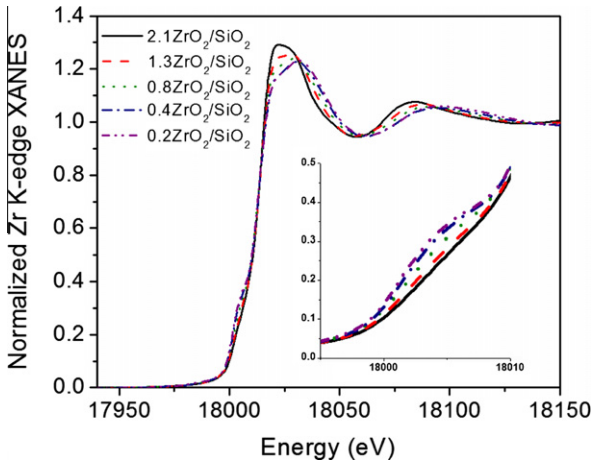

Fig. 2. Zr K-edge XANES after heating to 773 K in 10% O_2/He for 1 h at 4 K min^{-1}. Scans taken at ambient temperature in He. Inset is an enlargement of the pre-edge feature at 18,005 eV.

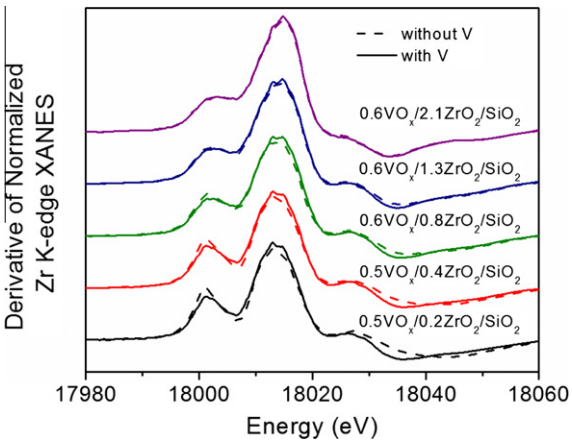

Fig. 3. Zr K-edge derivative spectra for samples with V (solid lines) and without V (dashed lines). Scans were taken at ambient temperature after heating to 773 K for 1 h in 10% O_2/He at 4 K min^{-1}.

on the surface interacting with the grafted V. The highest weight loading of Zr, 2.1 Zr nm^{-2}, showed the smallest change because it had the highest Zr/V ratio. The decrease in the peak intensity at 18.001 keV indicates that zirconium increases its coordination as a result of V grafting, possibly becoming centrosymmetric, as discussed elsewhere. The changes in the Zr K-edge spectra with Zr surface coverage indicate that some of the V interacts with Zr atoms bonded to the silica surface. A similar effect was observed in Ti K-edge spectra of $VO_x/TiO_2/SiO_2$ catalysts containing isolated vanadate species [4].

The Zr K-edge EXAFS spectra in Fig. 4 show a large peak centered at 1.35 Å, associated with backscattering from neighboring oxygen atoms approximately 2 Å from the Zr atoms. This peak decreases with increasing Zr surface density, which is most likely a result of two or more Zr—O path lengths whose backscattering destructively interferes and reduces the overall intensity. For the lowest Zr surface density, Zr is fully dispersed and likely contains a single shell of oxygen atoms with similar Zr—O bond distances; however, as the Zr loading increases, Zr begins to form higher coordinated structures. A similar reduction intensity is observed in tetragonal ZrO_2, which contains two Zr—O path lengths at 2.08 and 2.36 Å [34]. The backscattered waves from these two paths interfere causing the decrease in the intensity of the Zr—O peak observed in the EXAFS data shown in Fig. 4. The broadening in the sample spectra with increasing Zr surface density also implies that multiple O backscattering at increasing distances is the cause of the decrease in intensity and the O peak position shifts in the direction of the Zr—O backscattering for *m*-ZrO_2, also shown in Fig. 4. For all samples except that with the highest Zr surface density, the EXAFS spectra reveal weak Zr—Zr backscattering at slightly below 3 Å corresponding Zr—Zr path length of ~3.3 Å. At the highest Zr surface density, a signal appears consistent with backscattering from Zr atoms separated by 3.6 Å, as observed in *t*-ZrO_2. Attempts to fit the spectra were unsuccessful because of the variety of Zr environments and the limited data range.

The V K-edge XANES spectra (see Supplementary information) for all the catalysts investigated, as well as a reference spectrum of VO_x/SiO_2, are qualitatively similar, exhibiting a large pre-edge feature and an edge energy at 5483 eV characteristic of V^{5+} [3,4]. The V K-edge pre-edge feature at 5470 eV results from excitation of a vanadium 1s electron into a hybrid O-p and V-d orbital present in tetrahedral and pseudo-tetrahedral V oxides [38]. Examination of the derivative spectra presented in Fig. 5 reveals subtle changes with Zr loading. The shoulder at 5468 eV of the pre-edge feature decreases at the same time that the intensity of the main pre-edge peak increases with increasing Zr loading. This trend has been

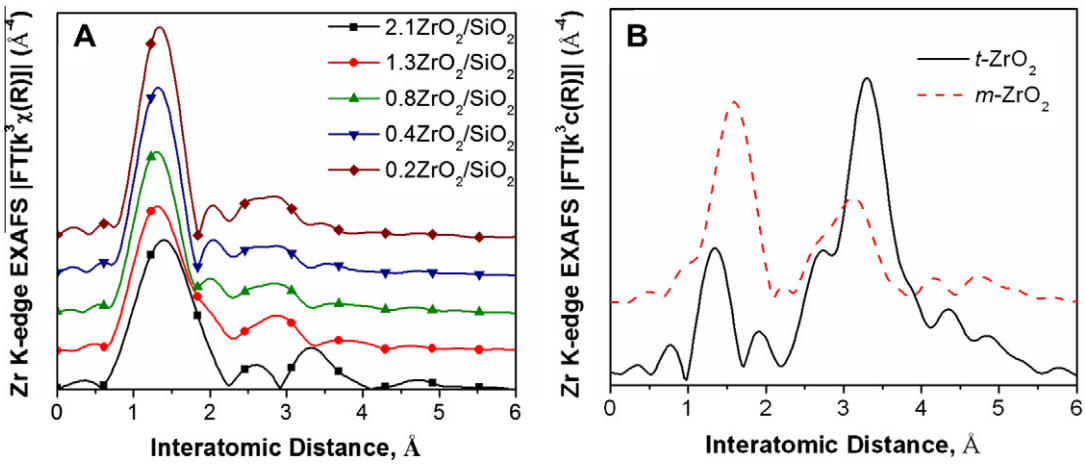

Fig. 4. Magnitude of Fourier-transformed Zr K-edge EXAFS spectra of selected samples (A) and simulated spectra of *t*-ZrO_2 and *m*-ZrO_2 (B). Samples were treated in 10% O_2/He at 773 K for 1 h before cooling in He and acquiring the spectra at ambient temperature. Spectra offset for clarity.

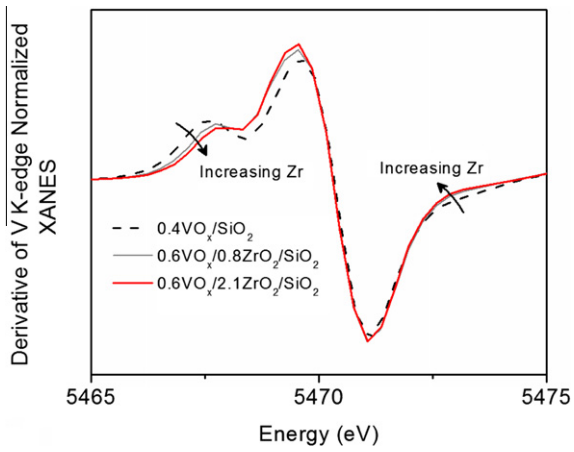

Fig. 5. Derivative of V K-edge normalized XANES. Samples were heated to 773 K in 60 cm^3 min^{-1} 10% O_2/He for 1 h at 4 K min^{-1} and then cooled in 60 cm^3 min^{-1} He to ambient temperature before taking scans. See Supporting information for normalized spectra.

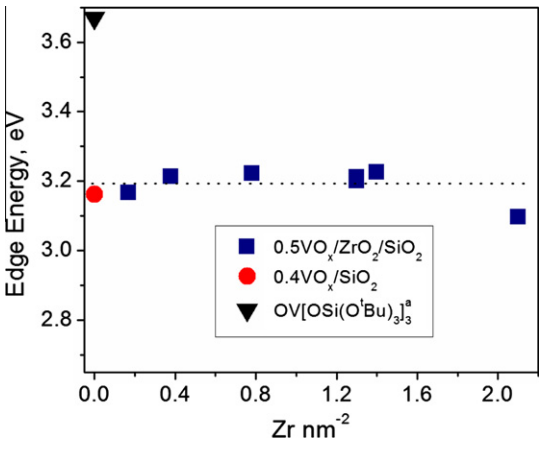

Fig. 7. UV–Vis edge energies of $VO_x/ZrO_2/SiO_2$ catalysts after treating in 20% O_2/N_2 to 723 K for 1 h. Samples cooled to ambient temperature in He before taking scan. [a]Reference values obtained from Ref. [41].

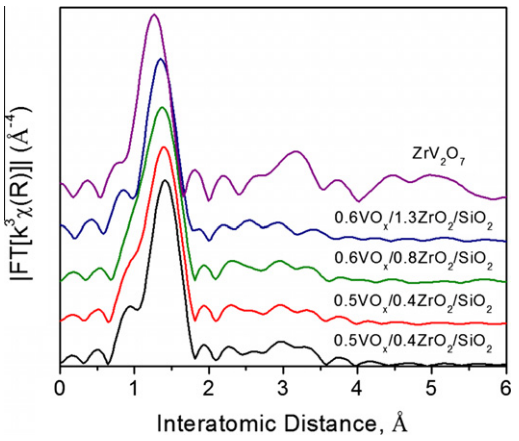

Fig. 6. Magnitude of Fourier-transformed k^3 weighted V K-edge EXAFS. Samples were heated to 773 K in 60 cm^3 min^{-1} 10% O_2/He for 1 h at 4 K min^{-1} and then cooled in 60 cm^3 min^{-1} He to ambient temperature before taking scans. The ZrV_2O_7 spectrum was simulated.

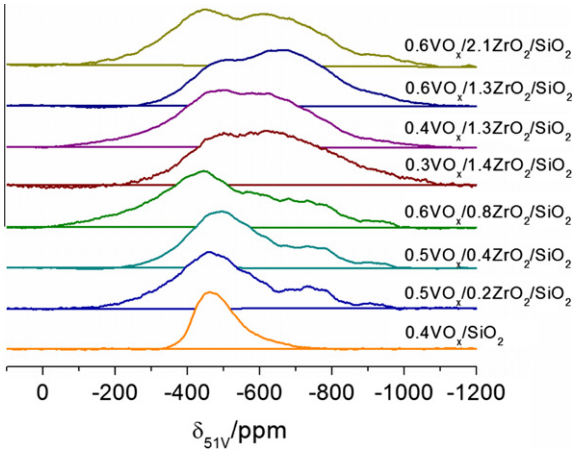

Fig. 8. ^{51}V MAS NMR of $VO_x/ZrO_2/SiO_2$ catalysts after treatment in 20% O_2/He at 773 K for 1 h and cooled to ambient temperature in He. Spectra were acquired on a 11.75 T magnet. V_2O_5 was used as the reference and set to −609 ppm.

observed previously and has been attributed to a narrowing of V—O bond length differences [38].

The V K-edge EXAFS data are shown in Fig. 6. All samples show a large peak associated with nearest neighbor oxygen backscattering that shifts slightly to smaller distances with increasing Zr surface coverage and in the direction of the V—O path found in ZrV_2O_7. A weak peak around 3 Å could indicate V—Zr interactions as seen in ZrV_2O_7; however, attempts to obtain information beyond the first shell through fitting were unsuccessful due to the variety of environments in which V is bound to the support.

The UV–Visible absorption edge energies determined for $VO_x/ZrO_2/SiO_2$ are shown in Fig. 7. Since bulk and silica-supported ZrO_2 has an edge energy above 4 eV, the optical transition is due to the ligand to metal charge transfer involving V [7,39,40]. All samples have edge energies that are higher than that observed for bulk V_2O_5 (2.05 eV), but smaller than that for $OV[OSi(O^tBu)_3]_3$ (3.65 eV) [41]. The observed edge energies are also consistent with the edge energy found for isolated O=VO_3 tetrahedra bound on silica [41]. The peak maxima for these samples of $VO_x/ZrO_2/SiO_2$ occur below 265 nm, consistent with what has been observed for isolated, tetrahedral O=VO_3 species as well [28]. The absence of a significant change in the edge energy with increasing Zr surface coverage also indicates that the electronic environment of vanadium remains essentially unchanged with increasing Zr loading.

^{51}V NMR spectra of the fully oxidized catalysts are shown in Fig. 8. The speed at which the sample rotated (7 kHz) was not sufficiently high to observe spinning sidebands for these samples. VO_x/SiO_2 shows a single peak at around −485 ppm characteristic of isolated vanadate species on silica [42,43]. Upon grafting Zr onto the sample, the −485 ppm peak broadens requiring a new Gaussian at −300 ppm to fit the data. This feature is most likely due to the presence of tetrahedral V sites weakly bound by one V—O—Zr bond [26,16]. A new peak is also observed at −750 ppm, characteristic of tetrahedrally coordinated V bound to the support by 3V—O—Zr bonds. Replacing Si with the less electronegative Zr will result in more electron density on the neighboring O and more negative chemical shifts [16]. This interpretation is supported by ^{51}V NMR spectra of ZrV_2O_7, which exhibit a large peak at −775 ppm [26,16,44]. As the surface density of Zr increases, an additional peak appears at approximately −650 ppm. A similar peak has been observed for vanadia supported on anatase and has been attributed to strongly bound vanadium in an octahedral environment involving a short V=O bond and a strong interaction with the support [16].

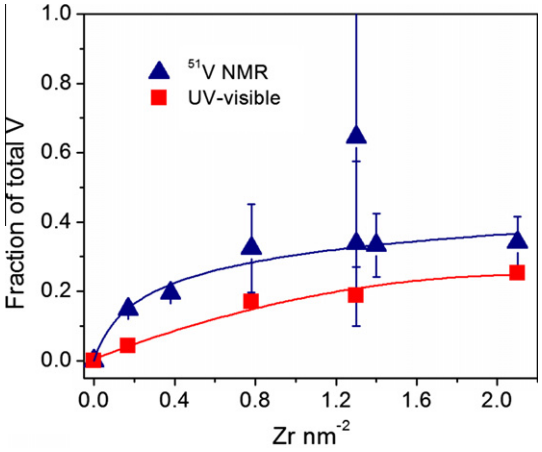

Fig. 9. Fraction of V—Zr sites on catalyst as determined by ^{51}V NMR peak fitting (blue trangles) and fraction of active sites as determined by UV–Vis (red squares). The errors indicate the 95% confidence interval from the fit. (For interpretation of the references to color in this figure legend, the reader is referred to the web version of this article.)

Gaussian peaks centered at −300, −485, −630, −750, and −930 ppm were fitted to each spectrum. The peak at −930 ppm is present in all samples and, with the peak at −300 ppm, suggests some octahedral V moieties on the surface [16,42]. Because the relative intensity of the peaks −630 and −750 ppm increased with increasing Zr loading, the areas of these peaks were divided by the total V signal to obtain a fraction of vanadium associated with zirconium. The ^{51}V spectrum of $0.3VO_x/1.4ZrO_2/SiO_2$ catalyst was also taken using a 300 MHz (7 T) magnet, and the resulting spectrum (see Supporting information) is the same as that taken at the higher field, indicating that the appearance of these signals is due to a true chemical shift and not to quadrupolar effects arising from V [17]. The results of the ^{51}V NMR peak fits are shown in Fig. 9. The NMR peak fitting indicates that the fraction of vanadium associated with zirconium increases with increasing zirconium surface coverage up to the point where ~35% of all V atoms are associated with Zr. The fraction for the 1.3 Zr nm^{-2} sample is significantly higher than the other samples, but this is likely due to the uncertainty in the fit of that spectrum. The 95% confidence interval for the fit is shown as error bars in Fig. 9, confirming the larger error for the $0.6VO_x/1.3ZrO_2/SiO_2$ sample. This particular sample also exhibited a very intense Raman peak at 924 cm^{-1} indicative of V—O—M bonds. The appearance of an unusually intense Raman peak near 924 cm^{-1} may be due to an anomaly in the synthesis procedure, as noted above. In fact, the other two samples synthesized with a similar Zr surface coverage in Table 1 showed V—Zr fractions similar to what would have be expected based on the trends with the remaining samples.

The spectroscopic results indicate that the $VO_x/ZrO_x/SiO_2$ catalysts prepared for this study consist primarily of O=V(O—Si)$_3$ and O=V(O—Zr)$_n$(O—Si)$_{3-n}$ (n = 1–3) units. The position of the chemical shift and the Zr agglomeration evidenced in the Zr K-edge XAS suggest that the total number of V with 1 or 2V—O—Zr bonds is small and that the dominant V structures on the catalyst are O=V(O—Si)$_3$ and O=V(O—Zr)$_3$; however, species with n = 1, 2 cannot be ruled out. In both cases, the vanadium atoms occur in pseudo-tetrahedral structures. It is notable, though, that while no differences could be observed in the electronic properties between the two types of sites by either UV–Visible spectroscopy or V K-edge XANES, the presence of O=V(O—Si)$_3$ and O=V(O—Zr)$_3$ species could be detected by ^{51}V NMR. As discussed elsewhere, the structural and electronic similarities between the two V environments have implications for the mechanism by which methanol oxidation occurs.

3.2. Studies of methanol oxidation

For low conversions from methanol to formaldehyde, the rate of methanol oxidation over supported vanadium catalysts was described by the following rate expression [1,4,5,45]

$$\frac{r_{app}}{[V]_{total}} = k_{app}[\mathrm{MeOH}]. \quad (1)$$

Here, r_{app} is the rate of formaldehyde formation, k_{app} is the apparent rate constant, $[V]_{total}$ is the total number of V atoms, and [MeOH] is the gas-phase concentration of methanol. Using Eq. (1), the apparent rate constant was determined from temperature-programmed reaction (TPRx) experiments. Representative TPRx results for sample $0.6VO_x/0.8ZrO_2/SiO_2$ are shown in the Supporting Information.

Fig. 10 shows that the apparent rate constant at 543 K increases by over an order of magnitude as the Zr surface coverage increases from 0 to 2.1 Zr nm^{-2}. This pattern is similar to that observed previously for $VO_x/TiO_2/SiO_2$ [4]. The apparent activation energy for methanol synthesis was determined from an Arrhenius plot of the rate of formaldehyde formation versus temperature. Fig. 11 shows that the apparent activation energy is 23 kcal/mol for VO_x/SiO_2 [3] but then decreases to 16 kcal/mol for a Zr coverage of 0.2 Zr/nm^2 and remains approximately constant for higher Zr coverages. It is also noted that apparent activation energy is essentially the same for all samples of $VO_x/ZrO_2/SiO_2$ and nearly identical to the value for ZrV_2O_7. The activation energies for $VO_x/ZrO_2/SiO_2$ are also similar to values reported earlier for ZrO_2-supported vanadia [1,27].

The data presented in Figs. 10 and 11 suggest that the vanadate species are distributed between two classes: those that are bonded exclusively to silica and those that are bonded exclusively to the zirconia overlayer deposited on the surface of silica. The former are described by the structure O=V(O—Si)$_3$, whereas the latter are described most generally by O=V(O—Zr)$_n$(O—Si)$_{3-n}$ (n = 1–3). Since the surface structural data available for the latter species are insufficient to precisely determine the number of V—O—Zr bonds, we will assume that n = 3 for the balance of the discussion presented here, because the dominant structure is most likely O=V(O—Zr)$_3$ as discussed previously. Therefore, the apparent rate coefficient for methanol oxidation can be described by the relationship:

$$K_{app} = xk^0_{SiO_2}exp\left(-\frac{E_{SiO_2}}{RT}\right) + (1-x)k^0_{ZrO_2}exp\left(-\frac{E_{ZrO_2}}{RT}\right), \quad (2)$$

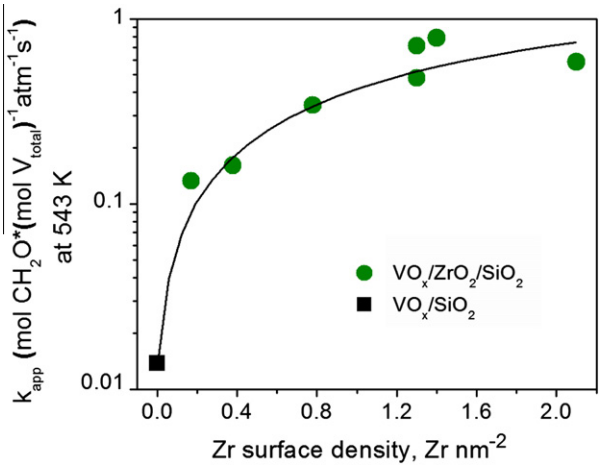

Fig. 10. Apparent rate constant for methanol oxidation over $VO_x/ZrO_2/SiO_2$ at 543 K as a function of Zr surface density.

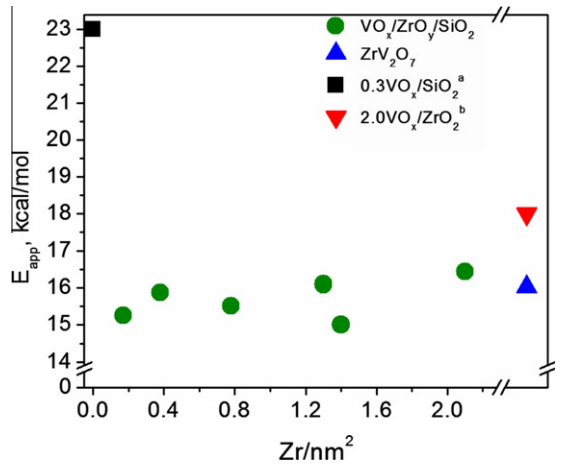

Fig. 11. Apparent activation energy for methanol oxidation on $VO_x/ZrO_2/SiO_2$ catalysts as a function of Zr surface coverage. [a,b]VO_x/SiO_2 and VO_x/ZrO_2 from Refs. [3,27], respectively.

where x is the fraction of vanadate sites bonded exclusively to SiO_2, $(1-x)$ is the fraction of sites bonded to ZrO_x exclusively, $K^0_{SiO_2}$ and $K^0_{ZrO_2}$ are the apparent pre-exponential factors for vanadate species bonded to SiO_2 and ZrO_x, respectively, and E_{SiO_2} and E_{ZrO_2} are the apparent activation energies for vanadate species bonded to SiO_2 and ZrO_x, respectively.

The intrinsic activity of the O=V(O—Zr)$_3$ species was obtained by dividing the values of k_{app} for $VO_x/ZrO_2/SiO_2$ reported in Fig. 10 by the fraction of V bound to Zr determined from the ^{51}V NMR spectra. In so doing, it was assumed that the contribution of O=V(O—Si)$_3$ species to the value of k_{app} is small, which, as will be shown below, is fully justified [3]. Fig. 12 shows that the apparent first-order rate coefficient attributed O=V(O—Zr)$_3$ species is nearly constant with Zr surface coverage. It is also noted that the magnitude of this apparent rate coefficient is two orders of magnitude higher than that for O=V(O—Si)$_3$ species, fully justifying the assumption made in preparing Fig. 12.

The number of O=V(O—Zr)$_3$ species was quantified independently using UV–Visible spectroscopy by counting the number of reduced vanadia centers after reduction in methanol at 600 K. This

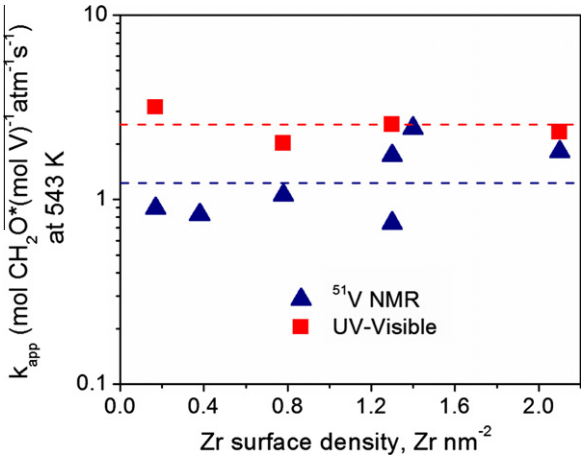

Fig. 12. Apparent rate constant as a function of Zr surface coverage normalized by the fraction of V strongly bound to Zr as determined by ^{51}V NMR peak fits (blue triangles) and normalized by the fraction of V reduced by MeOH at 600 K as determined by UV–Visible (red squares). Dashed lines are to guide the eye. (For interpretation of the references to color in this figure legend, the reader is referred to the web version of this article.)

temperature coincides with the peak in formaldehyde productivity for the catalysts prepared with Zr present but not for VO_x/SiO_2, which only becomes active at higher temperatures [see Supporting Information]. Since formaldehyde production proceeds in the absence of O_2, treatment in methanol at 600 K should only reduce the sites active for formaldehyde production given the lack of significant side reactions. Therefore, only the reduced sites determined by UV–Visible spectroscopy are considered to be active for methanol oxidation at 600 K on $VO_x/ZrO_2/SiO_2$ in the presence of O_2. The conversion from the measured oxygen uptake to the number of reduced V was made assuming $4e^-$ per O_2 consumed and that all reduced V was in the 4+ oxidation state. Justification for this assumption is given below. Fig. 9 shows that the fraction of all V sites that are catalytically active determined on the basis of UV–Visible spectroscopy in combination with pulsed reoxidation (see Experimental Section) is consistently lower than that determined independently from ^{51}V NMR. However, given the significant errors associated with both methods of site determination, the differences may not be physically significant. The important thing to note is that the fraction of active sites determined by UV–Visible spectroscopy also shows an increase with increasing Zr surface coverage, which further supports the claim that vanadia to bonded zirconia is responsible for the observed increase in catalytic activity. Consistent with the preceding discussion, it is seen in Fig. 12 that the value of the apparent rate coefficient attributable to O=V(O—Zr)$_3$ species determined from the analysis of UV–Visible data is nearly a factor of 2 higher than that determined from the analysis of ^{51}V NMR data.

The pre-exponential factor, $k^0_{ZrO_2}$, was calculated using both the NMR and UV–Visible method for determining the fraction of V present as O=V(O—Zr)$_3$ species. In the first approach, the values for the pre-exponential factor and activation energy for VO_x/SiO_2 were obtained from Bronkema et al. [27], and the activation energy for the VO_x/ZrO_2 sites was taken to be 16 kcal/mol, as measured in this study. The resulting pre-exponential factor was 6×10^6 and 3×10^6 $(atm\ s)^{-1}$ based on the site fractions determined from the UV–Visible and the ^{51}V NMR data, respectively. The second method that assumed the contribution to the rate by VO_x/SiO_2 sites was negligible. The resulting pre-exponential factor, with an activation energy of 16 kcal/mol, were 6×10^6 and 3×10^6 $(atm\ s)^{-1}$ for UV–Visible and ^{51}V NMR site fractions, respectively. Regardless of the method used, the pre-exponential factors obtained were comparable with those reported previously for isolated vanadate species present on VO_x/ZrO_2 [7×10^6 $(atm\ s)^{-1}$] [27]. This analysis suggests that the primary contribution to the higher rate of formaldehyde production on O=V(O—Zr)$_3$ sites relative to O=V(O—Si)$_3$ sites is the lower activation energy on the former type of site.

It is useful to review what is known about the mechanism of methanol oxidation and the influence of support composition before discussing possible reasons for the differences in the activity of O=V(O—Si)$_3$ species and O=V(O—Zr)$_3$ species. Both experimental and theoretical studies suggest that for isolated vanadate species supported on silica (i.e., O=V(O—Si)$_3$ species) methanol oxidation occurs via the mechanism shown in Fig. 13A [3,9,46]. Reaction begins with the adsorption of CH_3OH across a V—O—Si bond to form V—OCH_3 and Si—OH groups (Reaction 1). This process is quasi-equilibrated and is followed by the rate-limiting step in which an H atom is transferred from the methyl group of V—OCH_3 to the V=O bond (Reaction 2), resulting in the formation of adsorbed CH_2O, which quickly desorbs, and a V—OH group. In the next step, H_2O is formed via the condensation of the Si—OH and V—OH groups (Reaction 3). This leaves the V in the +3 oxidation state. Rapid reoxidation then restores V to the +5 state. Theoretical analyses of the elementary steps shown in Fig. 13a have confirmed that Reaction 1 is quasi-equilibrated, that Reaction 2 is the rate-limiting step, and that the reoxidation of V is much more rapid

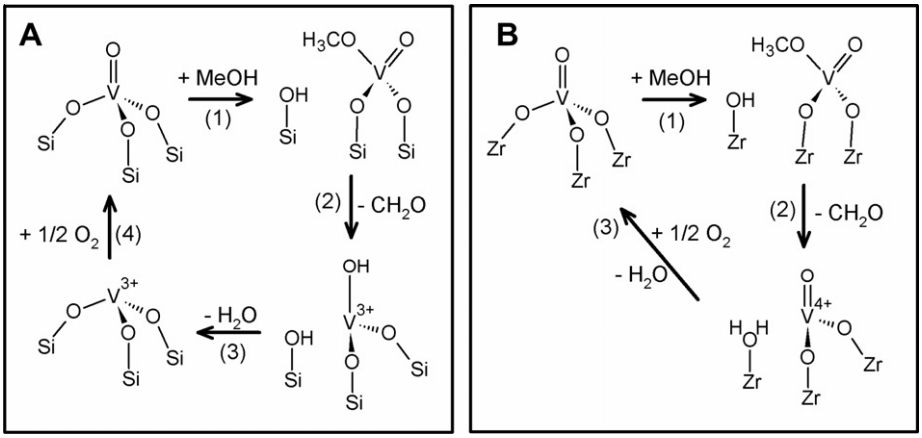

Fig. 13. Proposed schematic for methanol oxidation on VO_x/SiO_2 sites (A) and on VO_x/ZrO_2 sites (B).

than V reduction. These studies have also shown that the rate parameters obtained for the proposed mechanism are in close agreement with those determined experimentally [3,9].

Several attempts have been made to explain the observed dependence of the rate of methanol oxidation on support composition. Wachs and coworkers have proposed that the Sanderson electronegativity of the support metal cation affects the rate of methanol oxidation by influencing the adsorption of methanol (Reaction 1 in Fig. 13A) [2]. While the turnover frequency for methanol oxidation is found to increase with decreasing Sanderson electronegativity, both experimental and theoretical studies show no significant effect of support composition on the heat of methanol adsorption [1,4,5]. For methanol oxidation on $VO_x/TiO_2/SiO_2$, it has been proposed that larger domain sizes and greater electron delocalization of the titania layer result in a higher TOF toward formaldehyde; however, the manner in which electron delocalization affects the reaction kinetics was not defined [10].

Theoretical studies have suggested that the high activity of isolated vanadate species supported on titania may be due to the influence of O vacancies present at the support surface or to a change in the reaction mechanism relative to that shown in Fig. 13A. In the first of these two proposals, it is proposed that O vacancies occur adjacent to a few percent of the vanadate species supported on titania [4,5]. While the presence of the vacancy has minimal effect on the calculated equilibrium constant for methanol adsorption, the activation barrier for H-abstraction from V—OCH_3 groups (Reaction 2 in Fig. 13A) decreases by 7 kcal/mol relative to that for vanadate species that are not adjacent to an O vacancy. The reason for the decrease in activation energy is that the defect provides the active site with more flexibility, thereby allowing for a larger degree of H bonding in the product between Ti—OH and V—OH ligand species. The rate parameters determined on the basis of the O vacancy hypothesis agree well with those measured for titania-supported vanadia. The proposed interpretation is supported by EPR measurements of small concentrations of Ti^{3+} cations present on TiO_2 [47] and VO_x/TiO_2 [5] and by the observation of a correlation between the turnover frequency for methanol oxidation and the energy required to form an O vacancy in the support [5].

A second explanation for the high activity of titania-supported vanadia is possibility that the rate-limiting step for methanol oxidation occurring on VO_x/TiO_2 and VO_x/SiO_2 is not the same. Recent theoretical studies of methanol oxidation on rutile-supported vanadate species suggest that the rate-limiting step is H-abstraction from V—OCH_3 via reaction with Ti—OH [11]. This elementary reaction is illustrated in Fig. 13B. The same authors have also examined the adsorption of methanol on rutile-supported VO_x and found that CH_3OH addition across the V—O—Ti bond to form V—OCH_3/Ti—OH and on the V=O to form HO—V—OCH_3 is equally possible [12]. In the latter case, the H-abstraction would produce a Ti—OH group on the surface during the rate determining step. While a detailed microkinetic analysis of methanol oxidation for rutile-supported vanadate species was not carried out, it is plausible that the rate-limiting step for the pathway shown in Fig. 13B is operative for VO_x/TiO_2 and explains the higher activity of vanadate groups supported on titania relative to silica.

We now turn to a discussion of possible reasons for the higher activity of $VO_x/ZrO_x/SiO_2$ compared with VO_x/SiO_2. None of the evidence presented in this study shows any indication for intrinsic differences in the electronic properties of O=V(O—Si)$_3$ and O=V(O—Zr)$_3$ species. However, the latter species can be identified by difference in shielding caused by Si versus Zr, as demonstrated by the ^{51}V NMR spectra presented in Fig. 8. This observation and the greater ease of methanol reduction in O=V(O—Zr)$_3$ species clearly demonstrate that there are two types of vanadate groups on $VO_x/ZrO_x/SiO_2$. Attempts to identify oxygen vacancies formed upon the reduction in the ZrO_2/SiO_2 supports used in the present study showed no evidence for O vacancy formation, as was observed for TiO_2/SiO_2 [15]; therefore, we do not expect O vacancies to contribute to the higher activity of vanadates species grafted to zirconia. Likewise, no evidence was seen in the present work for increased electron delocalization with increasing ZrO_2 domain sizes, which would have been evidenced by a decreasing edge energy in the UV–Visible [48]. This leads us to suggest that the differences in activity between $VO_x/ZrO_x/SiO_2$ are due to the difference in the rate-limiting step in methanol oxidation occurring on the two types of catalyst. We propose that the methanol oxidation proceeds via the mechanism shown in Fig. 13A for O=V(O—Si)$_3$ species present on VO_x/SiO_2 and $VO_x/ZrO_x/SiO_2$, and via the mechanism shown in Fig. 13B for O=V(O—Zr)$_3$ species present on $VO_x/ZrO_x/SiO_2$. In the latter case, we envision that the Zr—OH groups participating in the rate-limiting step occur on Zr atoms adjacent to the O=V(O—Zr)$_3$ species. We note further that in the mechanism shown in Fig. 13B, vanadium is reduced to the +4 state upon formation of formaldehyde and water, which is consistent with the assumption used to define the number of active vanadium sites associated with zirconia determined by the UV–Visible methods discussed elsewhere.

4. Conclusions

Characterization of $VO_x/ZrO_x/SiO_2$ prepared with Zr surface coverages between 0.0 and 2.1 Zr nm^{-2} demonstrates that zirconia is

dispersed on the silica support primarily in two-dimensional structures exhibiting increasing Zr—O—Zr coordination with increasing Zr surface coverage. By contrast, vanadium exists as well dispersed pseudo-tetrahedral O=V(O—Zr)$_3$ or O=V(O—Si)$_3$ species. For a fixed vanadium loading, the fraction of vanadium bound to zirconia increases from 0% to approximately 35% with increasing Zr loading. A similar fraction of V sites was found to be active for the production of formaldehyde at 600 K, a temperature too low for significant activity on VO_x/SiO_2. Therefore, the active site on these catalysts is proposed to consist of tetrahedral O=V(OZr)$_3$ species. The formaldehyde production rate for $VO_x/ZrO_x/SiO_2$ catalysts is constant with Zr surface density when normalized to the number of these sites determined from either ^{51}V NMR or UV–Visible spectroscopy, indicating that the increase in the reaction rate is due to an increase in concentration of highly active species on the surface. The apparent pre-exponential factor for methanol oxidation at O=V(O—Si)$_3$ and O=V(O—Zr)$_3$ species is essentially the same, but the apparent activation barrier is 7 kcal/mol smaller for the latter sites. Thus, the nearly hundred-fold higher turnover frequency for methanol oxidation on O=V(O—Zr)$_3$ versus O=V(O—Si)$_3$ is due to lower activation barrier associated with the former sites. We propose that this is due to a difference in the intrinsic activation barrier for the rate-limiting step on the two catalysts as described in Fig. 13.

Acknowledgements

We would also like to thank Prof. Jeffrey Reimer, Dr. Jian Feng, and Dr. Joel Stettler for their helpful discussions and for running a sample on their 7T NMR magnet. Portions of this research were carried out at the Stanford Synchrotron Radiation Lightsource, a national user facility operated by Stanford University on behalf of the U.S. Department of Energy, Office of Basic Energy Sciences. The SSRL Structural Molecular Biology Program is supported by the Department of Energy, Office of Biological and Environmental Research, and by the National Institutes of Health, National Center for Research Resources, Biomedical Technology Program.

Appendix A. Supplementary material

Supplementary data associated with this article can be found, in the online version, at doi:10.1016/j.jcat.2011.05.001.

References

[1] L.J. Burcham, E.I. Wachs, Catal. Today 49 (1999) 467–484.
[2] G. Deo, I.E. Wachs, J. Catal. 146 (1994) 323–334.
[3] J.L. Bronkema, A.T. Bell, J. Phys. Chem. C 111 (2007) 420–430.
[4] W.C. Vining, A. Goodrow, J. Strunk, A.T. Bell, J. Catal. 270 (2010) 163–171.
[5] A. Goodrow, A.T. Bell, J. Phys. Chem. C 112 (2008) 13204–13214.
[6] X.T. Gao, S.R. Bare, J.L.G. Fierro, I.E. Wachs, J. Phys. Chem. B 103 (1999) 618–629.
[7] X.T. Gao, J.L.G. Fierro, I.E. Wachs, Langmuir 15 (1999) 3169–3178.
[8] H.T. Tian, E.I. Ross, I.E. Wachs, J. Phys. Chem. B 110 (2006) 9593.
[9] A. Goodrow, A.T. Bell, J. Phys. Chem. C 111 (2007) 14753.
[10] E.I. Ross-Medgaarden, I.E. Wachs, W.V. Knowles, A. Burrows, C.J. Kiely, M.S. Wong, J. Am. Chem. Soc. 131 (2009) 680–687.
[11] H.Y. Kim, H.M. Lee, R.G.S. Pala, H. Metiu, J. Phys. Chem. C 113 (2009) 16083–16093.
[12] H.Y. Kim, H.M. Lee, H. Metiu, J. Phys. Chem. C 114 (2010) 13736–13738.
[13] B.S. Uphade, Y. Yamada, T. Akita, T. Nakamura, M. Haruta, Appl. Catal. A: Gen. 215 (2001) 137–148.
[14] K.A. Koyano, T. Tatsumi, Micro. Mater. 10 (1997) 259–271.
[15] J. Strunk, W.C. Vining, A.T. Bell, J. Phys. Chem. C 114 (2010) 16937.
[16] O.B. Lapina, D.F. Khabibulin, A.A. Shubin, V.V. Terskikh, Prog. Nucl. Mag. Res. Spect. 53 (2008) 128–191.
[17] Z. Gan, P. Gor'kov, T.A. Cross, A. Samoson, D. Massiot, J. Am. Chem. Soc. 124 (2002) 5634–5635.
[18] R.E. Jentoft, S.E. Deutsch, B.C. Gates, Rev. Sci. Instrum. 67 (1996) 2111–2112.
[19] M. Newville, J. Synchrotron Radiat. 8 (2001) 96–100.
[20] B. Ravel, M. Newville, J. Synchrotron Radiat. 12 (2005) 537–541.
[21] J. Tauc, in: J. Tauc (Ed.), Amorphous and Liquid Semiconductors, Plenum, London, 1974, p. 159.
[22] M.D. Argyle, K. Chen, E. Iglesia, A.T. Bell, J. Phys. Chem. B 109 (2005) 2414–2420.
[23] I.E. Wachs, B.M. Weckhuysen, Appl. Catal. A: Gen. 157 (1997) 67–90.
[24] B.A. Morrow, Spectroscopic Characterization of Heterogeneous Catalysts, Elsevier, New York, NY, 1990.
[25] X.T. Gao, S.R. Bare, J.L.G. Fierro, M.A. Banares, I.E. Wachs, J. Phys. Chem. B 102 (1998) 5653–5666.
[26] J.L. Male, H.G. Niessen, A.T. Bell, T.D. Tilley, J. Catal. 194 (2000) 431–444.
[27] J.L. Bronkema, A.T. Bell, J. Phys. Chem. C 112 (2008) 6404–6412.
[28] X.T. Gao, S.R. Bare, B.M. Weckhuysen, I.E. Wachs, J. Phys. Chem. B 102 (1998) 10842–10852.
[29] A. Feinberg, C.H. Perry, J. Phys. Chem. Solids 42 (1981) 513–518.
[30] S.C. Su, A.T. Bell, J. Phys. Chem. B 102 (1998) 7000–7007.
[31] D.I. Enache, E. Bordes-Richard, A. Ensuque, F. Bozon-Verduraz, Appl. Catal. A: Gen. 278 (2004) 93–102.
[32] R.C. Garvie, J. Phys. Chem. 82 (1978) 218–224.
[33] P. Li, I.W. Chen, J.E. Penner-Hahn, Phys. Rev. B. 48 (1993) 10063–10073.
[34] G. Mountjoy, D.M. Pickup, R. Anderson, G.W. Wallidge, M.A. Holland, R.J. Newport, M.E. Smith, Phys. Chem. Chem. Phys. 2 (2000) 2455–2460.
[35] I. Nakai, J. Akimoto, M. Imafuku, R. Miyawaki, Y. Sugitani, K. Koto, Phys. Chem. Miner. 15 (1987) 113–124.
[36] H. Jung, S.M. Paek, J.B. Yoon, J.H. Choy, J. Porous Mater. 14 (2007) 369–377.
[37] S.C. Moon, M. Fujino, H. Yamashita, M. Anpo, J. Phys. Chem. B 101 (1997) 369–373.
[38] J. Wong, F.W. Lytle, R.P. Messmer, D.H. Maylotte, Phys. Rev. B 30 (1984) 5596–5610.
[39] J.G. Bendoraitis, R.E. Salomon, J. Phys. Chem. 69 (1965) 3666.
[40] E.F. Lopez, V.S. Excribano, M. Panizza, M.M. Carnasciali, G.J. Busca, J. Mater. Chem. 11 (2001) 1891–1897.
[41] A. Khodakov, B. Olthof, A.T. Bell, E. Iglesia, J. Catal. 181 (1999) 205.
[42] H. Eckert, I.E. Wachs, J. Phys. Chem. 93 (1989) 6796–6805.
[43] O.B. Lapina, V.M. Mastikhin, A.V. Nosov, T. Beutel, H. Knozinger, Catal. Lett. 13 (1992) 203–212.
[44] C. Hudalla, H. Eckert, R. Dupree, J. Phys. Chem. C 100 (1996) 15986–15991.
[45] M. Badlani, I.E. Wachs, Catal. Lett. 75 (2001) 137–149.
[46] J. Dobler, M. Pritzsche, J. Sauer, J. Am. Chem. Soc. 127 (2005) 10861.
[47] M. Li, W. Hebenstreit, U. Diebold, A.M. Tyryshkin, M.K. Bowman, G.G. Dunham, M.A. Henderson, J. Phys. Chem. B 104 (2000) 4944.
[48] D. Masure, P. Chaquin, C. Louis, M. Che, M. Fournier, J. Catal. 119 (1989) 415.